Sentinel-1 Backscatter Assimilation Using Support Vector Regression or the Water Cloud Model at European Soil Moisture Sites

Dominik Rains, Hans Lievens, Gabriëlle J. M. De Lannoy, Matthew F. McCabe, Richard A. M. de Jeu, and Diego G. Miralles

***Abstract*— Sentinel-1 backscatter observations were assimilated into the Global Land Evaporation Amsterdam Model (GLEAM) using an ensemble Kalman filter. As a forward operator, which is required to simulate backscatter from soil moisture and leaf area index (LAI), we evaluated both the traditional water cloud model (WCM) and the support vector regression (SVR). With SVR, a closer fit between backscatter observations and simulations was achieved. The impact on the correlation between modeled and *in situ* soil moisture measurements was similar when assimilating the Sentinel data using WCM ($\Delta R = +0.037$) or SVR ($\Delta R = +0.025$).**

***Index Terms*— Data assimilation, radar backscatter, soil moisture, support vector regression (SVR).**

I. Introduction

SOIL moisture regulates the recharge in aquifers and influences runoff. Low values are associated with hydrological droughts, whereas high values can influence flood occurrence [1]. Soil moisture also affects plant growth, albedo, the emission of longwave radiation, and the partitioning of the available energy. As such it has a pivotal influence on the state of the biosphere [2].

Land surface models can provide spatiotemporally continuous soil moisture estimates, with their accuracy depending on model physics, resolution, and input data. Alternatively, soil moisture can be retrieved from satellites, typically from passive microwave (radiometer) or active (radar) sensors [3]. The Soil Moisture and Ocean Salinity (SMOS) and Soil Moisture Active Passive (SMAP) missions, launched in 2009 and 2015, respectively, were the first specifically dedicated to monitor soil moisture. Both satellites are in polar orbits and measure the land-surface emission in the L-band, at resolutions of ~40 km, and with a repeat cycle of ~3 days [4], [5]. Soil moisture can be retrieved using radar backscatter from e.g., the Advanced Scatterometer (ASCAT) [6] at similar spatial resolutions than with SMOS and SMAP. However, higher resolution retrievals from backscatter are possible with synthetic aperture radar (SAR) [7]. As such, the Sentinel-1 (S1) satellites, launched in 2014 (S1A) and 2016 (S1B), have already been used to retrieve soil moisture at e.g., pan-European scale [8] and over agricultural areas in Europe [9].

Just like soil moisture from models, satellite retrievals have their own uncertainties and drawbacks, including the reliance on a number of ancillary data. The direct assimilation of backscatter measurements into land surface models allows for combining the strength of spatiotemporal continuous model estimates with real-world observations in a consistent manner [10]. Specific examples showing a positive effect of radar backscatter assimilation on soil moisture simulations are given by [7], [11]. To do this effectively, forward simulations are required to map the surface state (e.g., vegetation, soil moisture, and surface roughness) from the model to the observation space (i.e., backscatter). An example of a forward operator, frequently used to simulate backscatter, is the radiative-transfer water cloud model (WCM) [12]. Here, we compare forward simulations from a semiempirical WCM implementation using a linear relationship between soil moisture and backscatter to analogous forward simulations based on support vector regression (SVR) [13]. We then show results from assimilating two years of S1 backscatter into the Global Land Evaporation Amsterdam Model (GLEAM) [14], [15], and the validation using a range of soil moisture sites across Europe. The aim of the study is therefore to study the potential of Sentinel-1 backscatter assimilation to improve modeled soil moisture, and to analyze the added value of data-driven methods (such as SVR) for forward simulations.

II. Methodology and Data

A. GLEAM Soil Moisture Estimates

GLEAM is designed to estimate land surface evaporation and soil moisture from remote sensing data [14]. The soil moisture is obtained from a multilayer water balance model

Manuscript received November 11, 2020; revised March 16, 2021; accepted April 6, 2021. Date of publication June 10, 2021; date of current version December 22, 2021. This work was supported by the Belgian Science Policy Office as part of the ET-Sense project within the STEREO III programme (contract SR/02/377). *(Corresponding author: Dominik Rains.)*

Dominik Rains is with the Hydro-Climate Extremes Laboratory (H-CEL), Ghent University, 9000 Ghent, Belgium, and also with the Earth Observation Science Group, Department of Physics and Astronomy, University of Leicester, Leicester LE1 7RH, U.K. (e-mail: dominik.rains@ugent.be).

Hans Lievens and Gabriëlle J. M. De Lannoy are with the Department of Earth and Environmental Sciences, Catholic University Leuven, 3001 Leuven, Belgium.

Matthew F. McCabe is with the Biological and Environmental Science and Engineering Division, King Abdullah University of Science and Technology, Thuwal 23955, Saudi Arabia.

Richard A. M. de Jeu is with VanderSat, 2011 Haarlem, The Netherlands.

Diego G. Miralles is with the Hydro-Climate Extremes Laboratory (H-CEL), Ghent University, 9000 Ghent, Belgium.

Digital Object Identifier 10.1109/LGRS.2021.3073484

and is computed for up to three soil layers, depending on the land cover.

Although GLEAM is usually applied globally at 0.25° resolution, [16] showed that it is well suited for high-resolution regional applications. Here, GLEAM v3 [15] was run at a daily temporal resolution and a spatial resolution of 1 km at a series of European soil moisture sites for the years 2018–2019 (with 2017 serving as a model-spinup period). The top-layer (10 cm) soil moisture was used to compute the backscatter simulations with either the WCM or SVR approach, enabling the assimilation of S1 backscatter and consequent update of the modeled top-layer soil moisture. Changes to the top layer were then propagated to the deeper layers by the GLEAM model itself.

Vertically uniform soil properties, such as wilting point, field capacity and porosity, as well as land cover fractions, were based on the setup by Martens *et al.* [16]. Regarding dynamic forcing, we used Clouds and the Earth's Radiant Energy System (CERES) net radiation [17], Multi-Source Weighted-Ensemble Precipitation (MSWEP) v2 precipitation [18], and Atmospheric Infrared Sounder (AIRS) v6 air temperature [19]. As a vegetation phenology descriptor, GLEAM uses vegetation optical depth (VOD) from the Land Parameter Retrieval Model (LPRM, [20]). However, for the forward backscatter simulations with SVR or WCM, we used higher resolution 1 km cubic-spline interpolated ten-daily leaf area index (LAI) data retrieved from Proba-V observations and produced by the Copernicus Global Land Service [21] (see Section II-D).

B. Sentinel-1 Backscatter

We used ground range detected (GRD) S1 (A and B) observations from the Interferometric Wide Swath (IW) mode in VV polarization for 2018–2019. VV polarization was chosen over VH, as it is more sensitive to soil moisture [22]. Besides the standard S1 processing steps (i.e., precise orbit file application, thermal-noise correction, range-Doppler terrain correction, and radiometric calibration), systematic differences in the observations of the same pixel due to acquisitions being taken from different relative orbits were removed by bias correcting the static long-term mean backscatter [8]. For this, a longer data record was used (2014–2018) to allow for the computation of robust statistics. Among other effects, this normalizes the variation in backscatter caused by variable incidence angles, azimuth angles, and ascending/descending tracks. The original 20 m spaced observations were then resampled to the 1 km model resolution by means of averaging the backscatter in the linear domain (i.e., not in decibel). S1 observations were masked for freezing conditions (air temperature lower than 1.5 °C), snow cover (from the Interactive Multisensor Snow and Ice Mapping System [23]), and precipitation events larger than 40 mm/day. S1 outliers (larger/smaller than five standard deviations based on individual pixel statistics) were also removed.

C. Soil Moisture Measurements

To validate the soil moisture estimates from the GLEAM open-loop run (without data assimilation), as well as the impact of the S1 assimilation, *in situ* soil moisture measurements over Europe for 2018–2019 were obtained from the International Soil Moisture Network (ISMN, [24]). Only measurements within the first 10 cm soil depth were considered. In addition, soil moisture time series were individually quality controlled and those with obvious errors, such as constant values, were excluded (less than 5% of the data record). This procedure resulted in a total of 139 sites with each one having at least four months of soil moisture data for evaluation and at least 100 S1 observations for assimilation. Around 40% of these sites corresponded to croplands, 20% to tree cover, 15% each to herbaceous cover and grassland, and 10% to urban areas.

D. Water Cloud Model

In the WCM, the contribution from the soil can be estimated with a physics-based model [22] or e.g., by linear regression between backscatter and soil moisture [11]. Here, we adopted the latter, which required the calibration of two parameters that account for the sensitivity of the backscatter to either soil moisture (C, the aspect parameter) or surface roughness (D, the slope parameter). Two more parameters are required to account for vegetation scattering (A) and attenuation (B). In the WCM total backscatter σ^0 in decibel is computed as the sum of the backscatter from the soil σ^0_{soil} and vegetation σ^0_{veg}

$$\sigma^0 = \sigma^0_{\text{veg}} + t^2 \sigma^0_{\text{soil}}$$

with σ^0_{veg} characterized using a bulk vegetation descriptor V_1

$$\sigma^0_{\text{veg}} = A V_1 \cos\theta (1 - t^2)$$

and the vegetation attenuation t^2 estimated as

$$t^2 = \exp \frac{-2BV_2}{\cos\theta}$$

with V_2, a second bulk vegetation descriptor. The linear model to estimate bare soil backscatter is defined as

$$\sigma^0_{\text{soil}} = C + D\ \text{SM}_1$$

with SM_1 here referring to the upper 10 cm modeled soil moisture from GLEAM. SM_1 is expected to be temporally less variable and potentially biased compared to the more shallow soil layer actually observed by the S1 C-band. However, any bias was resolved through the calibration process, which was performed with data for 2018–2019 (the same time period as for the assimilation) from an open-loop run (see Section II-F for details on the ensemble generation). The calibration was performed in backscatter space, whereas the assimilation was evaluated in soil moisture space (see also [7], [11]). For both V_1 and V_2, we used the cubic-spline interpolated ten-day LAI retrievals from Proba-V. Using the temporally downscaled product allowed to increase the sample size of training data considerably, although other approaches of selecting the training data would certainly be possible. For θ, a fixed incidence angle of 40° was assumed, which corresponds approximately to the mean incidence angle of the normalized S1 observations. The parameters A, B, C, and D were optimized at each site

within a possible parameter space of [0, 5], [0, 10], [−35, 0], and [10, 60], respectively, [11]. The optimization focused on minimizing the root-mean-square difference (RMSD) between simulations and S1 VV observations [25]. For this, we chose the trust region reflective (TRF) algorithm. Using differential evolution optimization yielded very similar parameter values. The entire 2018–2019 period was chosen for the calibration to achieve a good generalization capability.

E. Support Vector Regression

As an alternative to the semiempirical WCM implementation described above, we explored the potential of SVR [13] as a forward operator. It has been shown that SVR can deal with the complex relationships between geophysical variables and microwave observations by e.g., [26]. SVR is capable of a high generalization and robustness in a variety of different applications, as well as a limited complexity in handling the learning phase. The SVR was trained to predict backscatter from the same two-year open-loop ensemble mean soil moisture and Proba-V LAI data used to calibrate the WCM at each site, once again by minimizing the RMSD between simulations and S1 observations. The hyperparameter optimization was performed using grid-search and a fivefold cross-validation to avoid overfitting. For the kernel parameter γ and the cost parameter C, possible values of [0.001, 0.01, 0.1, 1, 10] and [0.001, 0.01, 0.1, 1, 10, 20, 30, 40, 50, 100] were considered, respectively. The ϵ parameter, determining the maximum allowable error, was set to 0.1. To facilitate the regression, input data were mapped into a higher dimensional kernel feature space by nonlinear mapping through a radial basis kernel (RBF)

$$K(x, y) = \exp(-\gamma\,||x-y||^2)$$

with x encompassing soil moisture and LAI and y being the corresponding backscatter observations. In the training phase, both soil moisture and LAI were rescaled to match a distribution with zero mean and unit variance, preventing one variable (here LAI) from dominating the predictions due to a naturally larger variance. The same per-site scaling factors were applied later when performing the forward simulations during the data assimilation step.

F. Ensemble Kalman Filter

GLEAM was coupled to a deterministic ensemble Kalman filter [27]. To allow for a reasonable estimate of the model background error, GLEAM was run with 32 ensemble members; perturbations were added to each member based on [10]. Multiplicative log-normal perturbations (standard deviation = 0.3) were added to the precipitation. Air temperature was perturbed with additive normally-distributed noise (standard deviation = 2.5 °C) and net radiation was perturbed using random normal multiplicative noise (standard deviation = 0.3). Updates to the top-layer soil moisture were applied at each site separately by multiplying the innovation term (the difference between the local observation y and the nonlinear backscatter forward simulations from each ensemble member $h(x^b)$ with the Kalman gain K

$$x^a = x^b + K(y - h(x^b))$$

with x^a encompassing the soil moisture analysis for each ensemble member and x^b the soil moisture estimates prior to data assimilation. The Kalman gain was computed as

$$K = PH^{\intercal}(HPH^{\intercal} + R)^{-1}$$

where P is the uncertainty in soil moisture, H is the nonlinear forward operator $h(x^b)$ (WCM or SVR), and R is the observation error variance. For this study, R was calculated at each site based on the performance of the trained/calibrated SVR or WCM (i.e., as the mean-square difference between forward backscatter simulations and observations). The bias was implicitly removed by training/calibrating the SVR and WCM on a pixel-by-pixel basis.

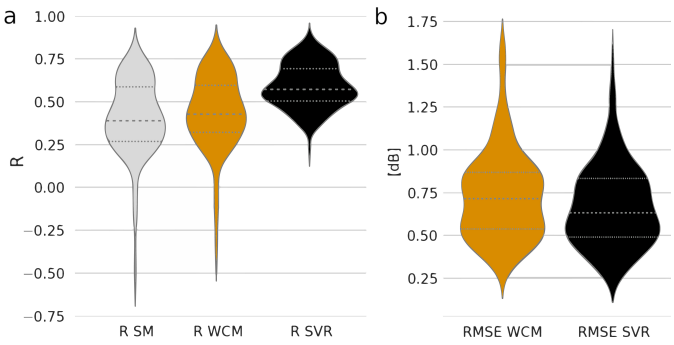

Fig. 1. For all ISMN sites: (a) R between GLEAM soil moisture and S1 backscatter observations, as well as between the WCM or SVR forward simulations and S1 backscatter. (b) RMSD between the WCM or SVR forward simulations and S1 backscatter.

III. Results

A. Assessment of Forward Simulations

To assess the performance of SVR and WCM, we compared the temporal Pearson correlation (R) between forward simulations and S1 backscatter [Fig. 1(a)]. SVR results in higher mean correlation ($\overline{R} = 0.59$) than WCM ($\overline{R} = 0.44$). For reference, the correlations between GLEAM soil moisture and S1 backscatter are also shown ($\overline{R} = 0.40$). Given that the relationship between forward simulations and observations might be nonlinear, we also examine the performance of SVR and WCM in terms of RMSD, which also acted as the objective function in the training/calibration phase [Fig. 1(b)]. Overall, SVR again performs better than WCM ($\overline{\text{RMSD}} = 0.67$ dB versus $\overline{\text{RMSD}} = 0.73$ dB). It is worth noting that for both sets of forward simulations, the average bias is quasi-zero, yet the variance is noticeably lower (0.29 dB for SVR, 0.25 dB for WCM) than for the observations (0.80 dB). The overall better performance of SVR may relate to its flexibility, i.e., not relying on a fixed model structure or assumptions, such as a linear relationship between soil moisture and backscatter. Fig. 2 shows example time series of S1 backscatter and WCM and SVR forward simulations for the SMOSMANIA Sabres (temperate cropland in southern France) and REMEDHUS Las Vacas (semiarid cropland in

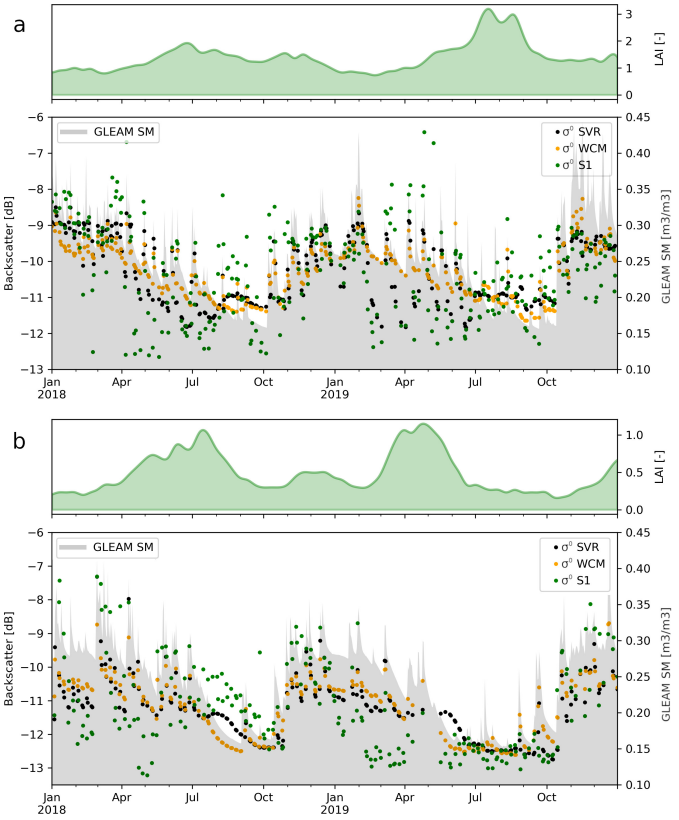

Fig. 2. Example time series of S1 observations and forward simulations from the WCM and SVR for (a) SMOSMANIA Sabres and (b) REMEDHUS Las Vacas sites. LAI (green area) and GLEAM soil moisture (gray area) were used to calibrate/train the WCM/SVR.

central Spain) sites. LAI and GLEAM open-loop soil moisture, the variables used to calibrate the WCM and train the SVR, are also shown. In general, the forward simulations are sensitive to precipitation spikes and soil moisture depletion. WCM simulations closely follow the soil moisture dynamics, while SVR simulations resemble to a higher degree the backscatter observations (see e.g., summer 2018). At the wetter Sabres site, the spring dry-down is well captured by SVR but not by WCM. However, both approaches struggle with replicating the very low backscatter during spring, also across other sites, suggesting an earlier seasonal dry-down than simulated. This is partly due to the simulated top 10 cm being less variable than the shallower soil layer observed by S1. Another reason might be the 1 km ten-daily interpolated LAI product not reflecting more localized vegetation dynamics.

B. Data Assimilation Impact

As a final step we assimilated the S1 observations into GLEAM. Assimilation runs, using SVR and WCM forward simulations, were compared to the open-loop and *in situ* soil moisture at ISMN sites (see Section II-C).

Fig. 3(a) shows the assimilation impact on terms of ΔR, i.e., the change in correlation between modeled and *in situ* soil moisture measurements across ISMN sites. For the majority of the 139 sites the assimilation improves the soil moisture simulations, especially when using SVR (67% versus 60% for WCM). Large changes, both positive and negative, are mostly limited to validation sites with shorter available records.

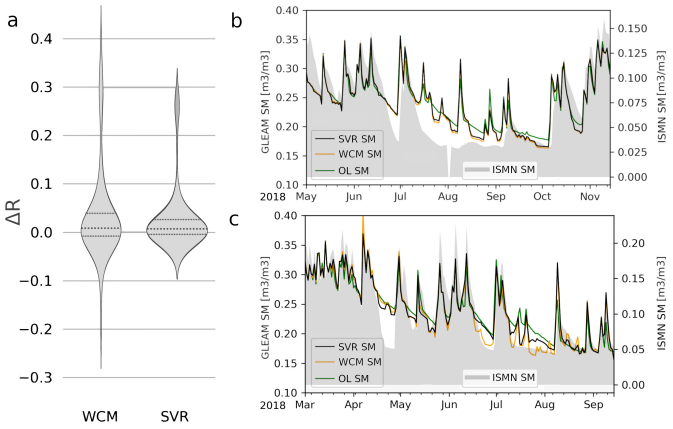

Fig. 3. (a) Distribution of the assimilation impact (ΔR) for all considered ISMN sites when using the WCM or SVR forward simulations. Temporal subset of soil moisture time series for the open-loop run and both assimilation experiments together with ISMN soil moisture for (b) Acqui Grandcal and (c) SMOSMANIA Sabres.

The overall impact of both SVR and WCM is, however, small ($\Delta R = +0.037$ for WCM, and $\Delta R = +0.025$ for SVR). We note that the validation was performed using all forecast and analysis steps (not only when S-1 observations were available). Improvements of such magnitude are consistent with those reported by Lievens *et al.* [7]. As mentioned, the observation error was directly based on the performance of the WCM or SVR predictions. Overall lower observation errors for the SVR experiment, in combination with smaller innovations due to the closer fit between forward simulations and observations, resulted in smaller soil moisture increments when compared to the WCM (0.005 m^3/m^3 versus 0.007 m^3/m^3).

To examine the results further, we highlight two particular sites that demonstrate the faster dry-out of the soil moisture observed by Sentinel-1. Fig. 3(b) shows the assimilation impact on soil moisture for a temporal subset at the Acqui Grandcal site (temperate tree cover). Here the ISMN *in situ* measurements are taken at 1 cm depth and the mentioned behavior is clearly visible. It is to a lesser extent visible at the nearby SMOSMANIA Sabres site Fig. 3(c), where the ISMN measurements are taken at 5 cm depth. In both cases, the assimilation partly steers the modeled soil moisture toward the *in situ* observations.

A detailed inspection of the assimilation impact across all sites showed no relationship with mean LAI, land cover or aridity (not shown). We therefore, attribute the differences in data assimilation performance across the sites mostly to the representativeness of point scale site measurements with respect to the observations and model data.

IV. Conclusion

We explored the potential of SVR as an observation operator for the assimilation of Sentinel-1 (S1) VV backscatter observations. To this end, GLEAM was run for 2018–2019 at soil moisture validation sites across Europe. The forward simulations from SVR yielded higher correlations with the backscatter from S1 than those from the frequently-used

WCM. Likewise, the RMSD between forward simulations and S1 backscatter was lower for SVR. Nevertheless, improvements to the upper layer soil moisture simulations were modest for both SVR and WCM experiments. This is in line with the results of the S1 backscatter assimilation by Lievens *et al.* [7]. A reduction in the innovations with SVR resulted in smaller increments, despite the smaller observation error calculated from the fit between forward operator simulations and observations. It was also shown that both sets of forward simulations underestimated the temporal variance of S1 backscatter. This might be due the first model layer being thicker (10 cm) than the penetration depth of the backscatter, or due to the lower variability in LAI at the model pixel scale. A more advanced selection of training data—e.g., using the same amount of samples from specific land surface conditions, such as soil moisture peaks and dry periods, or training/calibrating the SVR and WCM per season—should be explored in the future. Likewise, since [28] reported that the WCM can suffer from seasonal biases, the consideration of time-dependent errors could also be beneficial. Our findings show that data driven machine learning approaches, such as SVR, can be a viable alternative to semiempirical parameterized models with a fixed structure when assimilating backscatter observations. These approaches are capable of modeling high-dimensional behavior, yet special attention must be paid to potential overfitting which would merely replicate the observations and result in no assimilation impact. Here, this was prevented by training across two years with different LAI/soil moisture regimes as well as through fivefold cross-validation. Nonetheless, machine learning methods should in no way hinder the advancement of fully physical backscatter models but rather support and complement their development.

REFERENCES

[1] K. A. McColl, S. H. Alemohammad, R. Akbar, A. G. Konings, S. Yueh, and D. Entekhabi, "The global distribution and dynamics of surface soil moisture," *Nature Geosci.*, vol. 10, no. 2, pp. 100–104, Feb. 2017.

[2] J. K. Green *et al.*, "Large influence of soil moisture on long-term terrestrial carbon uptake," *Nature*, vol. 565, no. 7740, pp. 476–479, Jan. 2019.

[3] P. C. Dubois, J. van Zyl, and T. Engman, "Measuring soil moisture with imaging radars," *IEEE Trans. Geosci. Remote Sens.*, vol. 33, no. 4, pp. 915–926, Jul. 1995.

[4] D. Entekhabi *et al.*, "The Soil Moisture Active Passive (SMAP) mission," *Proc. IEEE*, vol. 98, no. 5, pp. 704–716, May 2010.

[5] Y. H. Kerr, P. Waldteufel, J.-P. Wigneron, J. Martinuzzi, J. Font, and M. Berger, "Soil moisture retrieval from space: The Soil Moisture and Ocean Salinity (SMOS) mission," *IEEE Trans. Geosci. Remote Sens.*, vol. 39, no. 8, pp. 1729–1735, Jun. 2001.

[6] W. Wagner *et al.*, "The ASCAT soil moisture product: A review of its specifications, validation results, and emerging applications," *Meteorol. Zeitschrift*, vol. 22, no. 1, pp. 5–33, Feb. 2013.

[7] H. Lievens *et al.*, "Joint Sentinel-1 and SMAP data assimilation to improve soil moisture estimates," *Geophys. Res. Lett.*, vol. 44, no. 12, pp. 6145–6153, Jun. 2017.

[8] M. El Hajj, N. Baghdadi, M. Zribi, and H. Bazzi, "Synergic use of Sentinel-1 and Sentinel-2 images for operational soil moisture mapping at high spatial resolution over agricultural areas," *Remote Sens.*, vol. 9, no. 12, p. 1292, Dec. 2017.

[9] B. Bauer-Marschallinger *et al.*, "Toward global soil moisture monitoring with Sentinel-1: Harnessing assets and overcoming obstacles," *IEEE Trans. Geosci. Remote Sens.*, vol. 57, no. 1, pp. 520–539, Dec. 2018.

[10] D. Rains, G. J. M. De Lannoy, H. Lievens, J. P. Walker, and N. E. C. Verhoest, "SMOS and SMAP brightness temperature assimilation over the Murrumbidgee basin," *IEEE Geosci. Remote Sens. Lett.*, vol. 15, no. 11, pp. 1652–1656, Nov. 2018.

[11] H. Lievens, B. Martens, N. E. C. Verhoest, S. Hahn, R. H. Reichle, and D. G. Miralles, "Assimilation of global radar backscatter and radiometer brightness temperature observations to improve soil moisture and land evaporation estimates," *Remote Sens. Environ.*, vol. 189, pp. 194–210, Feb. 2017.

[12] E. P. W. Attema and F. T. Ulaby, "Vegetation modeled as a water cloud," *Radio Sci.*, vol. 13, no. 2, pp. 357–364, Mar./Apr. 1978.

[13] V. Vapnik, *The Nature of Statistical Learning Theory*. Cham, Switzerland: Springer, 2013.

[14] D. G. Miralles, T. R. H. Holmes, R. A. M. De Jeu, J. H. Gash, A. G. C. A. Meesters, and A. J. Dolman, "Global land-surface evaporation estimated from satellite-based observations," *Hydrol. Earth Syst. Sci.*, vol. 15, no. 2, pp. 453–469, 2011.

[15] B. Martens *et al.*, "Gleam v3: Satellite-based land evaporation and root-zone soil moisture," *Geosci. Model. Develop.*, vol. 10, no. 5, pp. 1903–1925, 2017.

[16] B. Martens, R. de Jeu, N. Verhoest, H. Schuurmans, J. Kleijer, and D. Miralles, "Towards estimating land evaporation at field scales using GLEAM," *Remote Sens.*, vol. 10, no. 11, p. 1720, Oct. 2018.

[17] D. R. Doelling *et al.*, "Geostationary enhanced temporal interpolation for CERES flux products," *J. Atmos. Ocean. Technol.*, vol. 30, no. 6, pp. 1072–1090, 2013.

[18] H. E. Beck *et al.*, "MSWEP V2 global 3-hourly 0.1° precipitation: Methodology and quantitative assessment," *Bull. Amer. Meteorol. Soc.*, vol. 100, no. 3, pp. 473–500, Apr. 2019.

[19] H. H. Aumann *et al.*, "AIRS/AMSU/HSB on the Aqua mission: Design, science objectives, data products, and processing systems," *IEEE Trans. Geosci. Remote Sens.*, vol. 41, no. 2, pp. 253–264, Feb. 2003.

[20] Y. Y. Liu, R. A. M. de Jeu, M. F. McCabe, J. P. Evans, and A. I. J. M. van Dijk, "Global long-term passive microwave satellite-based retrievals of vegetation optical depth," *Geophys. Res. Lett.*, vol. 38, no. 18, 2011.

[21] A. Verger, F. Baret, and M. Weiss, "Near real-time vegetation monitoring at global scale," *IEEE J. Sel. Topics Appl. Earth Observ. Remote Sens.*, vol. 7, no. 8, pp. 3473–3481, Aug. 2014.

[22] A. K. Fung, "Microwave scattering and emission models and their applications," Tech. Rep., 1994.

[23] S. R. Helfrich, D. McNamara, B. H. Ramsay, T. Baldwin, and T. Kasheta, "Enhancements to, and forthcoming developments in the interactive multisensor snow and ice mapping system (IMS)," *Hydrol. Process.*, vol. 21, no. 12, pp. 1576–1586, 2007.

[24] W. A. Dorigo *et al.*, "The international soil moisture network: A data hosting facility for global *in situ* soil moisture measurements," *Hydrol. Earth Syst. Sci.*, vol. 15, no. 5, pp. 1675–1698, May 2011.

[25] N. Baghdadi, M. El Hajj, M. Zribi, and S. Bousbih, "Calibration of the water cloud model at C-band for winter crop fields and grasslands," *Remote Sens.*, vol. 9, no. 9, p. 969, Sep. 2017.

[26] D. Rains, R. Sabia, D. Fernandez-Prieto, M. Marconcini, and T. Katagis, "Extended analysis of SMOS salinity retrieval by using support vector regression (SVR)," in *Proc. IEEE Geosci. Remote Sens. Symp.*, Jul. 2014, pp. 2265–2268.

[27] G. Evensen, "The ensemble Kalman filter: Theoretical formulation and practical implementation," *Ocean Dyn.*, vol. 53, no. 4, pp. 343–367, Nov. 2003.

[28] D. Shamambo, B. Bonan, J.-C. Calvet, C. Albergel, and S. Hahn, "Interpretation of ASCAT radar scatterometer observations over land: A case study over southwestern France," *Remote Sens.*, vol. 11, no. 23, p. 2842, Nov. 2019.